entropy

IMPACT FACTOR 2.7

Indexed in: PubMed

CITESCORE 4.7

Article

Practical Real-Time Phase Drift Compensation Scheme for Quantum Communication Systems

Xiaotian Song, Chunsheng Zhang, Dong Pan, Min Wang, Jianxing Guo, Feihao Zhang and Guilu Long

Special Issue

New Advances in Quantum Communication and Networks

Edited by

Prof. Dr. Guilu Long

MDPI

https://doi.org/10.3390/e25101408

entropy

MDPI

Article

Practical Real-Time Phase Drift Compensation Scheme for Quantum Communication Systems

Xiaotian Song [1], Chunsheng Zhang [1], Dong Pan [1], Min Wang [1], Jianxing Guo [1], Feihao Zhang [1] and Guilu Long [1,2,3,4,*]

[1] Beijing Academy of Quantum Information Sciences, Beijing 100193, China; songxt@baqis.ac.cn (X.S.); zhangcs@baqis.ac.cn (C.Z.); pandong@baqis.ac.cn (D.P.); wangmin@baqis.ac.cn (M.W.); guojx@baqis.ac.cn (J.G.); zhangfh@baqis.ac.cn (F.Z.)
[2] State Key Laboratory of Low-Dimensional Quantum Physics and Department of Physics, Tsinghua University, Beijing 100084, China
[3] Frontier Science Center for Quantum Information, Beijing 100084, China
[4] Beijing National Research Center for Information Science and Technology, Beijing 100084, China
* Correspondence: gllong@mail.tsinghua.edu.cn

Abstract: Quantum communication systems are susceptible to various perturbations and drifts arising from the operational environment, with phase drift being a crucial challenge. In this paper, we propose an efficient real-time phase drift compensation scheme in which only existing data from the quantum communication process is used to establish a stable closed-loop control subsystem for phase tracking. This scheme ensures the continuous operation of transmission by tracking and compensating for phase drift in the phase-encoding quantum communication system. The experimental results demonstrate the effectiveness and feasibility of the proposed scheme with an average quantum bit error rate of 1.60% and a standard deviation of 0.0583% for 16 h of continuous operation.

Keywords: quantum communication; phase drift; real-time phase compensation

Citation: Song, X.; Zhang, C.; Pan, D.; Wang, M.; Guo, J.; Zhang, F.; Long, G. Practical Real-Time Phase Drift Compensation Scheme for Quantum Communication Systems. *Entropy* **2023**, *25*, 1408. https://doi.org/10.3390/e25101408

Academic Editor: Giuseppe Vallone

Received: 11 September 2023
Revised: 26 September 2023
Accepted: 29 September 2023
Published: 1 October 2023

1. Introduction

Quantum communication [1,2] is a field dedicated to achieving unconditional security between two legitimate parties, namely, Alice and Bob. Over the years, significant advancements have been made in both theoretical and experimental aspects [3–16], garnering considerable attention from diverse disciplines. Notably, the introduction of commercial single-photon level applications of quantum physics [17] has underscored the growing significance of practical quantum communication systems in real-world scenarios. However, it is crucial to acknowledge that real-world application environments are considerably more intricate and diverse compared to controlled laboratory settings. These complexities have the potential to impact system operations and even lead to disruptions.

Coupling with environment will adversely influence the performance of quantum systems [17,18]. Unlike laboratory environments where temperature control is commonly achieved through air conditioning and optical fiber channels are carefully arranged, the field environment lacks specialized environmental control measures and most fiber channels are installed on-site. The impact of field environments on quantum communication systems can be broadly categorized into two main aspects: polarization and phase drift. Polarization issues primarily arise from channel disturbances in installed fiber channels, while phase drift is often caused by interferometer drift. In phase-encoding quantum communication systems, polarization-related challenges can be effectively mitigated through ingenious system architecture design [4,19,20], in which long-term stability can be achieved without the need for polarization compensations. However, addressing phase drift requires careful consideration of operational conditions. Environmental isolation is one possible countermeasure, which reduces the speed of phase drift but increases system

complexity [21]. Another popular approach is the active feedback scheme, which has received significant attention. These schemes involve techniques such as using additional reference light for active alignment or performing pre-transmission phase drift parameter scanning [10]. However, such schemes often lead to a reduction in transmission efficiency. Machine learning techniques [22] have also been employed to predict phase drift. However, a substantial amount of training data must be collected beforehand for accurate predictions. More recently, efficient schemes utilizing mismatched data [23] for calibration have emerged, although they still require additional data transmission.

In conclusion, phase drift in field environments poses significant challenges for phase-coding quantum communication systems. While innovative design approaches and active feedback schemes have been explored, further research is needed to enhance transmission efficiency and develop robust solutions for real-world applications. Here, we propose a practical real-time calibration scheme for phase tracking. In our scheme, the system can continuously run without any additional transmission efficiency reduction or information exchange process by a finely designed closed-loop control algorithm, which is validated in our subsequent experiment. Experimental results show that the phase-coding quantum communication system with our phase tracking scheme can be operated stably and continuously for 16 h with an average quantum bit error rate (QBER) of 1.60% and a standard deviation of 0.0583%.

2. Methods

In a practical phase coding four-state style quantum communication system [4,20], four phases 0, $\frac{\pi}{2}$, π, $\frac{3\pi}{2}$ should be randomly encoded at Alice and Bob's interferometers, respectively. Considering that most of the commercial phase modulators are based on lithium niobate ($LiNbO_3$), which has quite stable half-wave voltage and good modulation linearity under a certain modulation bandwidth [24,25], we assume a linear relationship between the driving voltage and the modulated phase. Additionally, the half-wave voltages at the phase modulators in Alice and Bob's interferometers are assumed to be constant and denoted as $V_{\pi Ac}$ and $V_{\pi Bc}$, respectively. Therefore, the driving voltages of the four phases can be obtained as

$$\begin{cases} V_{\frac{\pi}{2}A(B)} = V_{0A(B)} + \frac{1}{2}V_{\pi A(B)c} \\ V_{\pi A(B)} = V_{0A(B)} + V_{\pi A(B)c} \\ V_{\frac{3\pi}{2}A(B)} = V_{0A(B)} + \frac{3}{2}V_{\pi A(B)c} \end{cases}, \tag{1}$$

where $V_{0A(B)}$, $V_{\frac{\pi}{2}A(B)}$, $V_{\pi A(B)}$, $V_{\frac{3\pi}{2}A(B)}$ are the driving voltages of 0, $\frac{\pi}{2}$, π, $\frac{3\pi}{2}$ at Alice's (Bob's) side, respectively. In addition, $V_{0A(B)}$ can be considered as the reference voltage for the modulation voltages at Alice's (Bob's) phase modulator. From Equation (1), we can easily determine that the phase difference between Alice and Bob can be compensated by an additional driving voltage of $V = V_{0A} - V_{0B}$ on the phase modulator. Here, we take the asymmetric Faraday–Sagnac–Michelson interferometer (FSMI)-based quantum communication system [20] for example, and for convenience, we consider the case of interference peak in our analysis, as the non-interference peaks can be filtered out by gated-mode single-photon detector. According to the analysis in Ref. [26], the two outputs of the interferometer at Bob can be described as

$$\begin{aligned} P_{1\text{out}} &= P_d + \eta(1 - v\cos\Delta\varphi), \\ P_{2\text{out}} &= P_d + \eta(1 + v\cos\Delta\varphi), \end{aligned} \tag{2}$$

where P_d is the dark count probability of the single photon detector (SPD), η is the quantum efficiency of the photon, which satisfies $\eta \ll 1$, v is the interference fringe visibility of the interferometers, and $\Delta\varphi$ is the phase difference between Alice and Bob.

With different phase coding definitions of bit 0 and 1 at the two communication parties, the QBER can be given by

$$e = \frac{P_{1\text{out}}}{P_{1\text{out}} + P_{2\text{out}}} = \frac{P_d + \eta(1 - v\cos\Delta\varphi)}{2(P_d + \eta)} \tag{3}$$

or

$$e = \frac{P_{2\text{out}}}{P_{1\text{out}} + P_{2\text{out}}} = \frac{P_d + \eta(1 + v\cos\Delta\varphi)}{2(P_d + \eta)}. \tag{4}$$

It can be clearly seen that the formulas are symmetric and equivalent, so we just consider the first case for example. For simplicity, we define e_0 as the QBER when $\Delta\varphi = 0$:

$$e_0 = e(\Delta\varphi = 0) = \frac{P_d + \eta(1 - v)}{2(P_d + \eta)}, \tag{5}$$

and Equation (3) can be adjusted to be

$$\begin{aligned} \cos\Delta\varphi &= \frac{(1-2e)(P_d+\eta)}{\eta v} \\ &= \frac{(1-2e)(P_d+\eta)}{\eta(1 - \frac{2e_0(P_d+\eta) - P_d}{\eta})} \\ &= \frac{1-2e}{1-2e_0} \end{aligned}. \tag{6}$$

Further more, the incremental driving voltage that is needed for compensation can be calculated by

$$\begin{aligned} \Delta V_i &= \frac{V_\pi}{\pi}\Delta\varphi_i \\ &= \pm\frac{V_\pi}{\pi}\arccos\frac{1-2e_i}{1-2e_0} \end{aligned}', \tag{7}$$

where the subscript i means the parameter of the i-th round of transmission, and after considering the boundary conditions, e_i should satisfy with

$$e_i = \begin{cases} e_0, & 0 \le e_i \le e_0 \\ e_i, & e_0 < e_i < 0.5 \\ 0.5, & 0.5 \le e_i \le 1 \end{cases}. \tag{8}$$

From Equation (7), we can observe that, apart from the value of the driving voltage difference, the direction of voltage adjustment should be considered as well. Here, we define $\Delta e_i = e_i - e_{i-1}$ to roughly evaluate the correctness of the previous modulation direction, which is represented by ε_i, and thus determine whether to change the modulation direction for this time by

$$\varepsilon_i = \begin{cases} \varepsilon_{i-1}, & \Delta e_i \le 0 || i > 0 \\ -\varepsilon_{i-1}, & \Delta e_i > 0 || i > 0 \\ 1, & i = 0 \end{cases}. \tag{9}$$

Therefore, Equation (7) can be substituted with the subsequent formula

$$\Delta V_i = \varepsilon_i \frac{V_\pi}{\pi}\arccos\frac{1-2e_i}{1-2e_0}, \tag{10}$$

and the driving voltage value of the next round can be easily obtained by

$$V_{i+1} = V_i + \Delta V_i. \tag{11}$$

In order to achieve a more stable operation for the system, we also introduced the Proportional–Integral–Derivative (PID) algorithm to calibrate the driving voltage with

$$\Delta V_i' = K_P \Delta V_i + K_I \sum_{n=1}^{i} \Delta V_n + K_D(\Delta V_i - \Delta V_{i-1}), \tag{12}$$

where K_P, K_I, K_D are the coefficients of the PID algorithm, and Equation (7) can be adjust to be

$$V_{i+1} = V_i + \Delta V_i'. \tag{13}$$

To conclude, the main flowchart of the proposed scheme is illustrated in Figure 1.

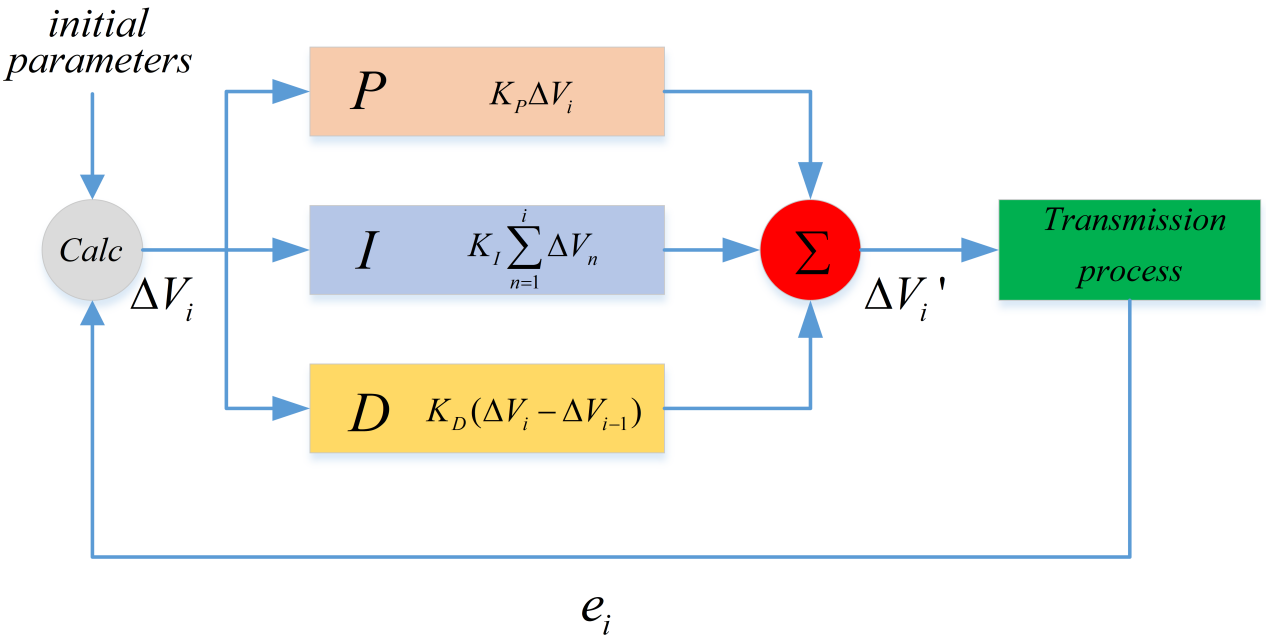

Figure 1. The main flowchart of the real-time phase drift compensation scheme. Calc, the calculation module to calculate the incremental driving voltage ΔV_i using the initial parameters and e_i; P, I, and D respectively represent the proportional, integral, and derivative components; $\sum$, sum of the three components.

3. Experiment and Results

We perform our scheme on an FSMI-based quantum communication system, as schematically shown in Figure 2. A fiber laser produces 1550 nm photon pulses with a width of 50 ps and a repetition frequency of 1.25 GHz; an intensity modulator attenuates the optical pulses to $\mu = 0.6$ photons per pulse combined with an attenuator. Benefiting from the sophisticated design of the FSMI, the polarization disturbance in the system need not be considered. The delay of the interferometers is 400 ps and both interferometers are equipped with a phase modulator on their long arms. The phase modulator has three drive voltage interfaces, two of which are RF interfaces for random phase modulation with a repetition frequency of 1.25 GHz and one is a direct current (DC) bias interface for phase compensation. A 12-bit digital-to-analog converter (DAC) is employed for phase tracking, allowing for a total range of 12V and providing a precision of 2.93 mV. The coded pulses are then sent to Bob over a 50 km fiber channel. After transmission, the photons pass through Bob's FSMI and finally detected by two InGaAs single photon detectors (SPDs), whose average detection efficiency, dark count rate, and afterpulse probability are 20 %, 1×10^{-6}, and 1.4 %, respectively. It should be noted that, before transmission, we obtain the initialization parameters and $e_0 = 1.59$ % (shown as Figure 3) through a scanning process.

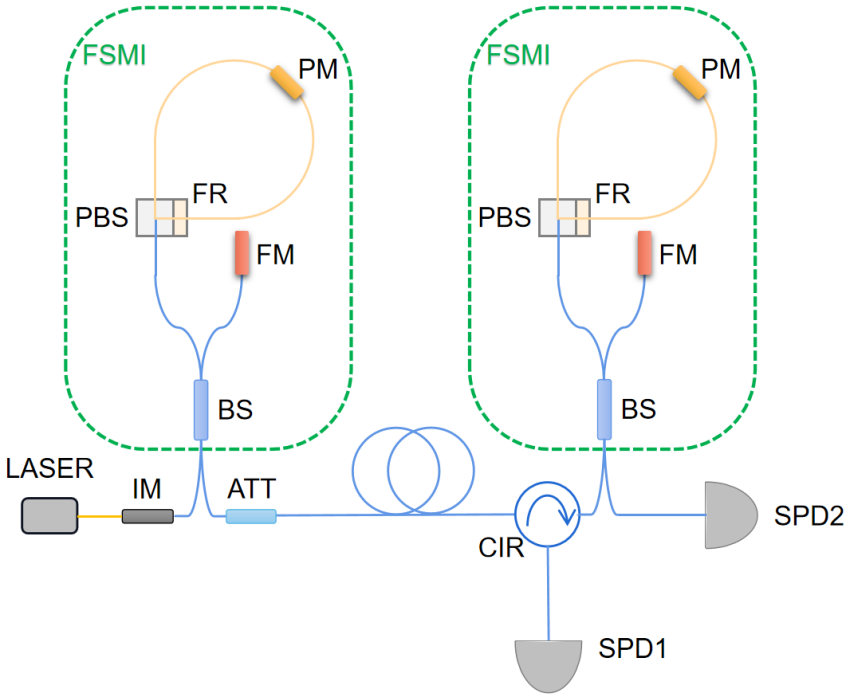

Figure 2. Schematic of the experimental setup. IM, intensity modulator; FSMI, asymmetric Faraday–Sagnac–Michelson interferometer; BS, beam splitter; FM, Faraday mirror; PBS, polarization beam splitter; FR, Faraday rotator; PM, phase modulator; ATT, attenuator; CIR, circulator; SPD, single-photon detector. The yellow lines represent polarization-maintaining fibers (PMFs), and the blue ones are single-mode fibers (SMFs).

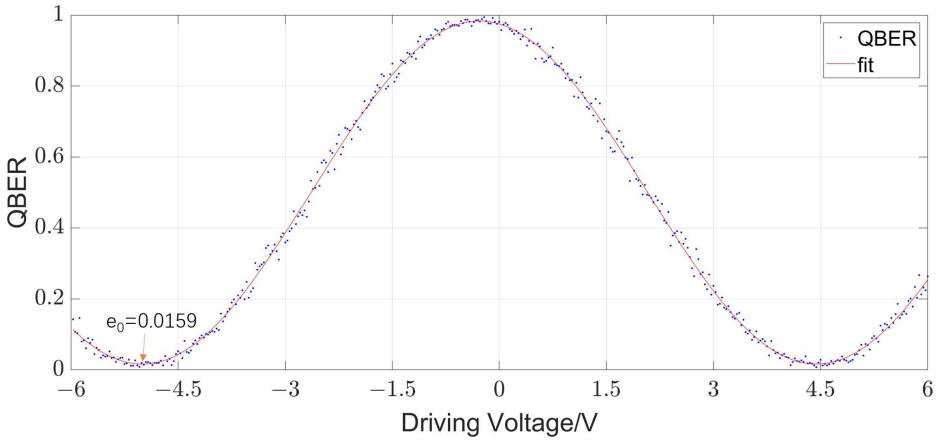

Figure 3. QBER verse Driving Voltage of the phase modulator.

To better simulate the complex field environments, a hot air fan is used to blow the interferometer for about half an hour, followed by a subsequent cooling treatment. Figure 4 depicts the experimental results obtained from running the system for 1 h. The results demonstrate a high overall stability of the system, with an average QBER value of 1.69% and a standard deviation of 0.0813%. However, a noticeable difference is still observed compared to the previously measured value e_0. Considering the rapid velocity of phase shift, in order to mitigate this discrepancy, we increase the frequency of feedback compensation from 1 s to 0.1 s per iteration. Figure 5 illustrates the test results under similar experimental conditions as before, showing a distinct decrease in QBER. The average value and standard deviation reached 1.62% and 0.0687%, respectively. Moreover, the standard deviation decreased to 0.0425% when performing statistical calculations at a rate of every 1 s. This result validates the effectiveness of improving the feedback speed in enhancing

the overall system performance. It should be noted that both sets of experimental results exhibit noticeable periodic fluctuations in QBER, primarily occurring during full-cycle voltage adjustments due to limited driving voltage. This is mainly attributed to insufficient modulation bandwidth of the modulation electrode and its temperature-dependent half-wave voltage drift. The limited modulation bandwidth results in a longer time required for the modulator to reach the target value. During this period, the optical pulses passing through the modulator are subjected to inaccurate modulation. Additionally, the inaccuracy in the half-wave voltage directly leads to errors in the modulation voltage. Both of these situations can cause an instantaneous increase in the QBER.

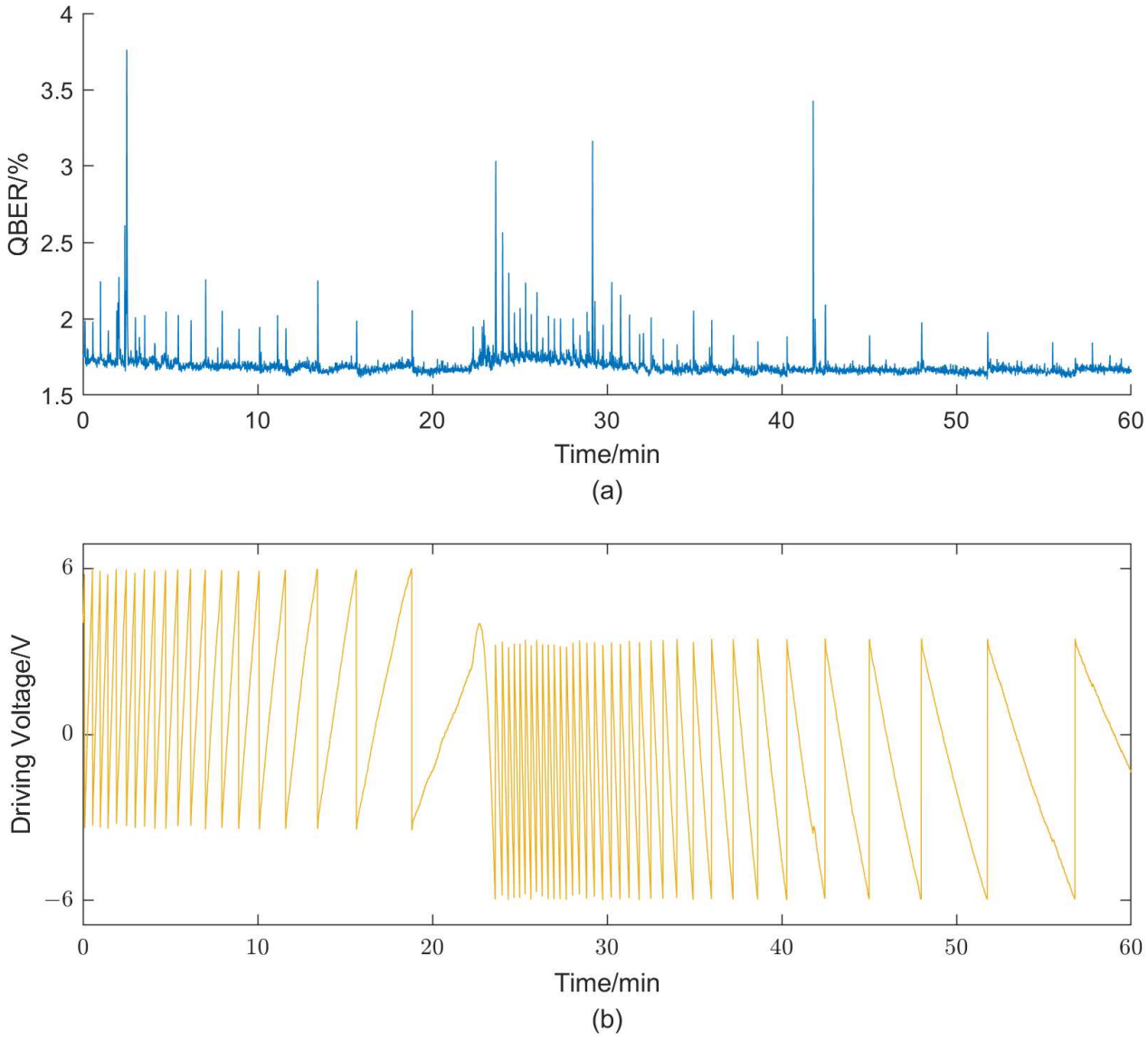

Figure 4. Obtained QBER (**a**) and driving voltage of the phase modulator (**b**) with a feedback compensation frequency of 1 s per iteration.

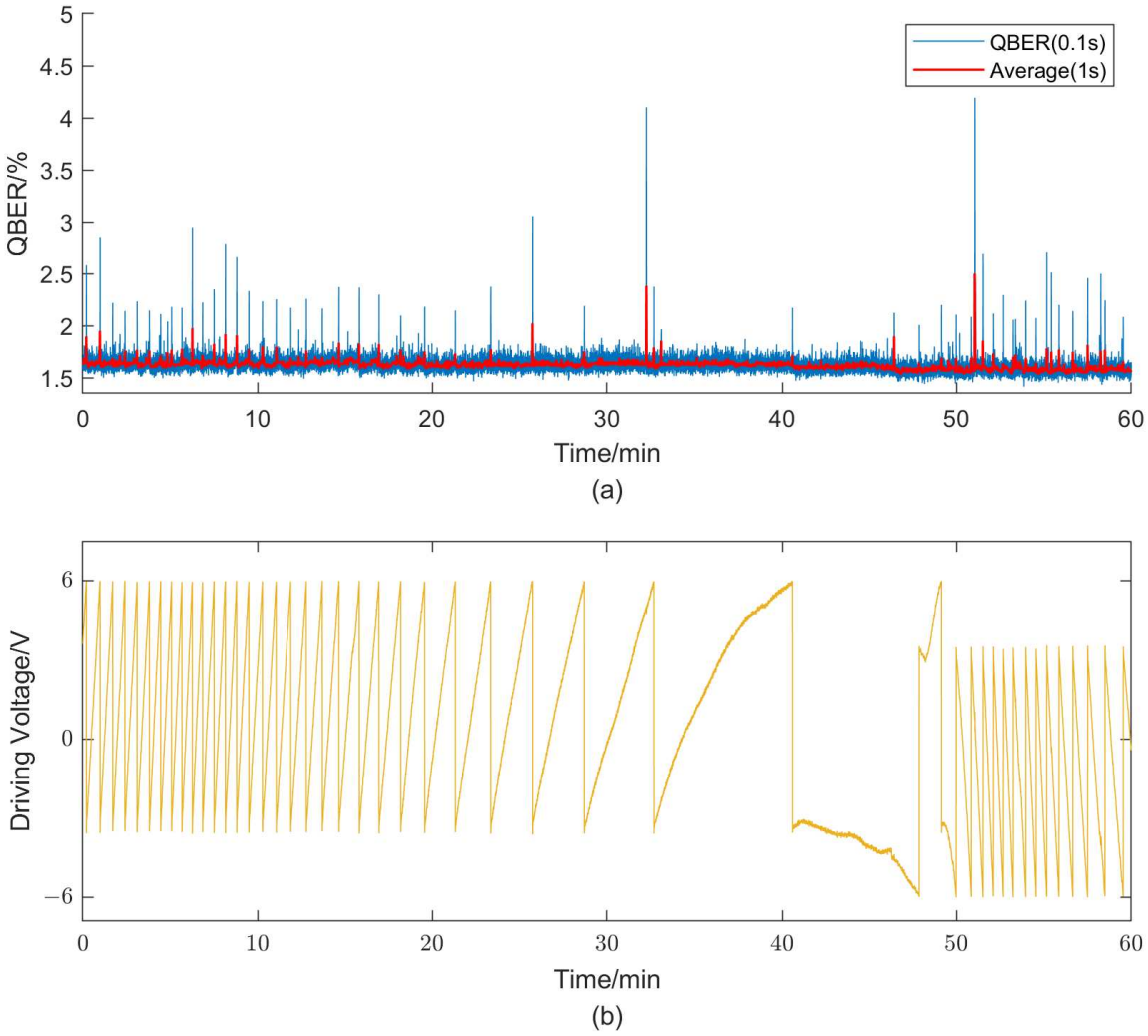

Figure 5. Obtained QBER (**a**) and driving voltage of the phase modulator (**b**) with a feedback compensation frequency of 0.1 s per iteration.

To further validate the long-term stability of the system, we conduct an extended stability test lasting nearly 16 h with a feedback compensation frequency of 0.1 s per iteration. Figure 6 presents the QBER, its statistical distribution, and the variations in feedback driving voltage. The obtained QBER achieves an average value of 1.60% and a standard deviation of 0.0583%.

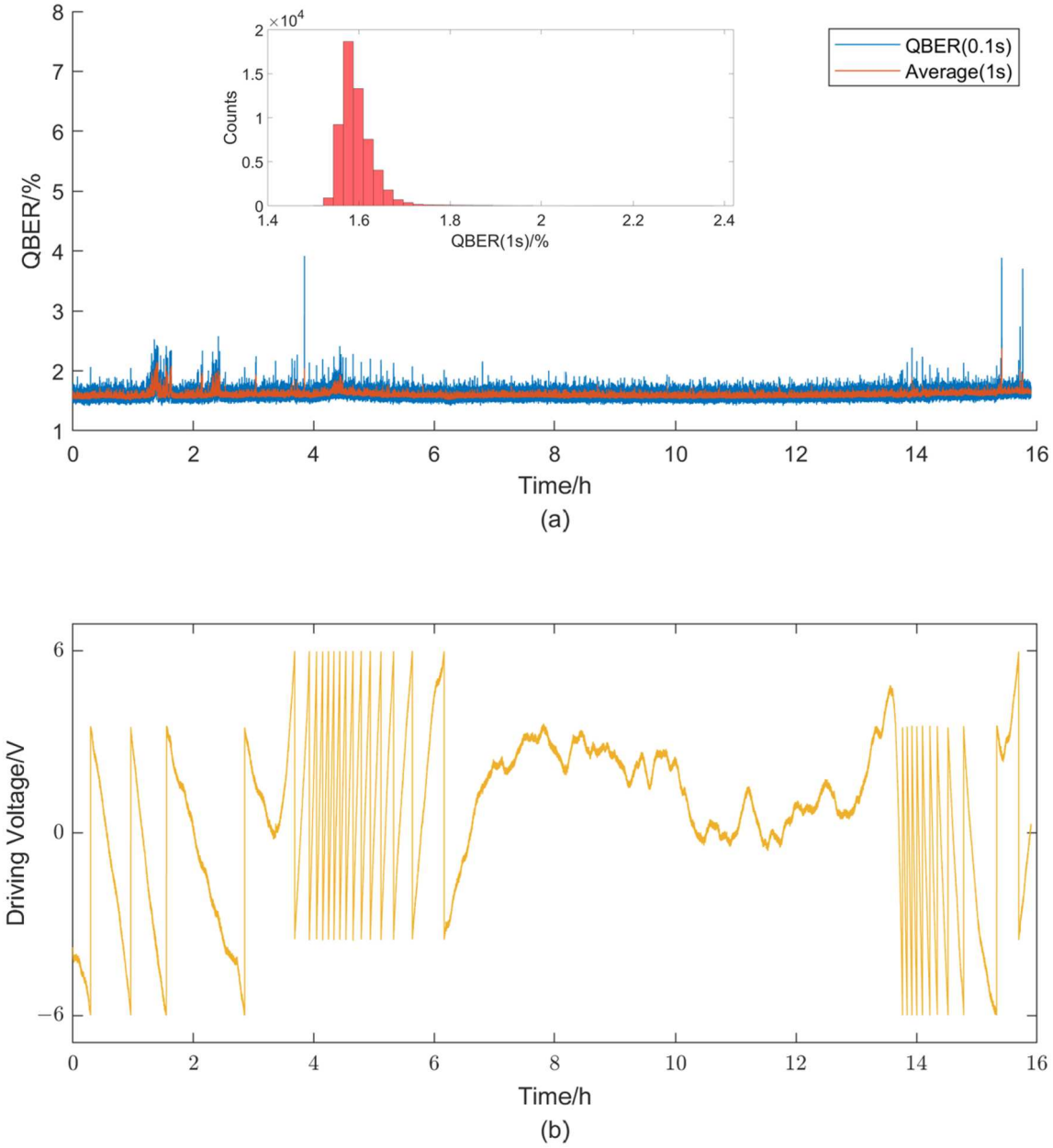

Figure 6. QBER, its statistical distribution (**a**), and driving voltage of the phase modulator (**b**) with a feedback compensation frequency of 0.1 s per iteration for 16 h.

4. Conclusions

In this paper, we propose a real-time phase drift compensation scheme for phase-coding quantum communication systems, in which only existing data from the quantum communication process is used to establish a stable closed-loop control subsystem for phase tracking without any additional transmission efficiency reduction or information exchange process. Our scheme is applied into an FSMI-based phase-coding quantum communication system, leading to a stable and continuous operation, even with a complex environmental disturbance. Note that, in our long-term stability experiment, we obtain an average QBER value of 1.60%, which is approximately equal to e_0 = 1.59%, and the effectiveness of our scheme has been effectively validated. Additionally, it can be observed from the experimental results that increasing the statistical frequency can effectively improve system

performance. However, this also results in a reduced number of statistical samples, leading to larger statistical errors. Therefore, a careful balance is needed in this regard, especially when the repetition rate is lower, which results in relatively smaller counts and larger fluctuations. Another point that needs to be mentioned is that, during the phase tracking process, there is still a possibility of incorrect modulation direction due to sudden phase changes or statistical fluctuations when the phase tracking driving voltage operates near the target value. Consequently, the incorrect modulation direction results in a higher QBER, which is a clear indication of modulation direction errors and can be quickly corrected through subsequent compensation, leading to a relatively stable state. The stability of the experimental results also verifies this point.

Author Contributions: Conceptualization, X.S., C.Z. and G.L.; methodology, X.S. and C.Z.; software, J.G. and F.Z.; validation, X.S., C.Z., D.P. and M.W.; formal analysis, X.S.; data curation, X.S. and C.Z.; writing—original draft preparation, X.S.; writing—review and editing, G.L., D.P., X.S., M.W., F.Z. and C.Z.; supervision, G.L. All authors have read and agreed to the published version of the manuscript.

Funding: This research was funded by the China Postdoctoral Science Foundation (2022M710401); National Natural Science Foundation of China (12205011); and the Young Elite Scientists Sponsorship Program by the China Association for Science and Technology (2022QNRC001).

Institutional Review Board Statement: Not applicable.

Data Availability Statement: No new data were created or analyzed in this study. Data sharing is not applicable to this article.

Conflicts of Interest: The authors declare no conflict of interest.

References

1. Bennett, C.H.; Brassard, G. Quantum cryptography: Public key distribution and coin tossing. In Proceedings of the IEEE International Conference on Computers, Systems and Signal Processing, Bangalore, India, 9–12 December 1984.
2. Long, G.L.; Liu, X.S. Theoretically efficient high-capacity quantum-key-distribution scheme. *Phys. Rev. A* **2002**, *65*, 032302. [CrossRef]
3. Long, G.L.; Zhang, H. Drastic increase of channel capacity in quantum secure direct communication using masking. *Sci. Bull.* **2021**, *66*, 1267. [CrossRef] [PubMed]
4. Song, X.T.; Wang, D.; Lu, X.M.; Huang, D.J.; Jiang, D.; Li, L.X.; Fang, X.; Zhao, Y.B.; Zhou, L.J. Phase-coding quantum-key-distribution system based on Sagnac–Mach-Zehnder interferometers. *Phys. Rev. A* **2020**, *101*, 032319. [CrossRef]
5. Scarani, V.; Renner, R. Quantum Cryptography with Finite Resources: Unconditional Security Bound for Discrete-Variable Protocols with One-Way Postprocessing. *Phys. Rev. Lett.* **2008**, *100*, 200501. [CrossRef] [PubMed]
6. Gottesman, D.; Lo, H.-K.; Lutkenhaus, N.; Preskill, J. Security of quantum key distribution with imperfect devices. *Quantum Inf. Comput.* **2004**, *4*, 325.
7. Peev, M.; Pacher, C.; Alléaume, R.; Barreiro, C.; Bouda, J.; Boxleitner, W.; Debuisschert, T.; Diamanti, E.; Dianati, M.; Dynes, J.F.; et al. The SECOQC quantum key distribution network in Vienna. *New J. Phys.* **2009**, *11*, 075001. [CrossRef]
8. Lo, H.K.; Curty, M.; Qi, B. Measurement-device-independent quantum key distribution. *Phys. Rev. Lett.* **2012**, *108*, 130503. [CrossRef]
9. Lucamarini, M.; Yuan, Z.L.; Dynes, J.F.; Shields, A.J. Overcoming the rate–distance limit of quantum key distribution without quantum repeaters. *Nature* **2018**, *557*, 400–403. [CrossRef]
10. Yuan, Z.L.; Shields, A.J. Continuous operation of a one-way quantum key distribution system over installed telecom fibre. *Opt. Express* **2005**, *13*, 660–665. [CrossRef]
11. Kwek, L.C.; Cao, L.; Luo, W.; Wang, Y.; Sun, S.; Wang, X.; Liu, A.Q. Chip-based quantum key distribution. *AAPPS Bull.* **2021**, *31*, 15. [CrossRef]
12. Wang, C. Quantum secure direct communication: Intersection of communication and cryptography. *Fundam. Res.* **2021**, *1*, 91–92. [CrossRef]
13. Chen, Z.; Sun, Z.; Pei, Y.; Yin, L. Generalized sparse codes for non-Gaussian channels: Code design, algorithms, and applications. *Fundam. Res.* **2022**, *2*, 284–295. [CrossRef]
14. Gao, C.Y.; Guo, P.L.; Ren, B.C. Efficient quantum secure direct communication with complete Bell-state measurement. *Quantum Eng.* **2021**, *3*, e83. [CrossRef]
15. Zhang, H.R.; Sun, Z.; Qi, R.; Yin, L.; Long, G.-L.; Lu, J. Realization of quantum secure direct communication over 100 km fiber with time-bin and phase quantum states. *Light. Sci. Appl.* **2022**, *11*, 83. [CrossRef] [PubMed]
16. Zhou, Z.Y.; Zhu, Z.H.; Shi, B.S. Diffractive Theory Study of Twisted Light's Evolution during Phase-Only OAM Manipulations. *Quantum Eng.* **2023**, *2023*, 4589181. [CrossRef]

17. Nicolas, G.; Grégoire, R.; Wolfgang, T.; Hugo, Z. Quantum cryptography. *Rev. Mod. Phys.* **2002**, *74*, 145.
18. Zhang, F.H.; Xing, J.; Hu, X.; Pan, X.; Long, G. Coupling-selective quantum optimal control in weak-coupling NV-13 C system. *AAPPS Bull.* **2023**, *33*, 2. [CrossRef]
19. Mo, X.F.; Zhu, B.; Han, Z.F.; Gui, Y.Z.; Guo, G.C. Faraday—Michelson system for quantum cryptography. *Opt. Lett.* **2005**, *30*, 2632–2634. [CrossRef]
20. Wang, S.; Chen, W.; Yin, Z.Q.; He, D.Y.; Hui, C.; Hao, P.L.; Fan, Y.G.J.; Wang, C.; Zhang, L.J.; Kuang, J.; et al. Practical gigahertz quantum key distribution robust against channel disturbance. *Opt. Lett.* **2018**, *69*, 2030–2033. [CrossRef]
21. Kimura, T.; Nambu, Y.; Hatanaka, T.; Tomita, A.; Kosaka, H.; Nakamura, K. Single-photon interference over 150 km transmission using silica-based integrated-optic interferometers for quantum cryptography. *Jpn. J. Appl. Phys.* **2004**, *9*, 1217–1219. [CrossRef]
22. Liu, J.Y.; Ding, H.J.; Zhang, C.M.; Xie, S.P.; Wang, Q. Practical Phase-Modulation Stabilization in Quantum Key Distribution via Machine Learning. *Phys. Rev. Appl.* **2019**, *12*, 014059. [CrossRef]
23. Wang, D.; Song, X.T.; Zhou, L.J.; Zhao, Y.B. Real-time phase tracking scheme with mismatched-basis data for phase-coding quantum key distribution. *IEEE Photonics J.* **2020**, *12*, 1–7. [CrossRef]
24. Wooten, E.L.; Kissa, K.; Yi-yan, A.; Murphy, E.J.; Lafaw, D.A.; Hallemeier, P.F.; Maack, D.; Attanasio, D.V.; Fritz, D.J.; Mcbrien, G.; et al. A Review of Lithium Niobate Modulators for Fiber-Optic Communications Systems *IEEE J. Sel. Top. Quantum Electron.* **2000**, *6*, 69–82. [CrossRef]
25. Wang, C.; Zhang, M.; Chen, X.; Bertrand, M.; Shams-Ansari, A.; Chandrasekhar, S.; Winzer, P.; Lončar, M. Integrated lithium niobate electro-optic modulators operating at CMOS-compatible voltages. *Nature* **2018**, *562*, 101–104. [CrossRef] [PubMed]
26. Kulik, S.P.; Molotkov, S.N. Decoy state method for quantum cryptography based on phase coding into faint laser pulses. *Laser Phys. Lett.* **2017**, *14*, 125205. [CrossRef]